Journal of Physics: Condensed Matter

Study of rutile TiO_2(110) single crystal by transient absorption spectroscopy in the presence of Ce^{4+} cations in aqueous environment. Implication on water splitting

To cite this article: K Katsiev and H Idriss 2024 *J. Phys.: Condens. Matter* **36** 325002

OPEN ACCESS
IOP Publishing
Journal of Physics: Condensed Matter
J. Phys.: Condens. Matter **36** (2024) 325002 (9pp)
https://doi.org/10.1088/1361-648X/ad4763

Study of rutile TiO_2(110) single crystal by transient absorption spectroscopy in the presence of Ce^{4+} cations in aqueous environment. Implication on water splitting

K Katsiev[1] **and H Idriss**[2,*]

[1] Surface Science and Advanced Characterization, SABIC-CRD at KAUST, Thuwal 23955, Saudi Arabia
[2] Institute of Functional Interfaces (IFG), Karlsruhe Institute of Technology (KIT), 76344 Eggenstein-Leopoldshafen, Germany

E-mail: hicham.idriss@kit.edu

Received 4 March 2024, revised 25 April 2024
Accepted for publication 3 May 2024
Published 17 May 2024

Abstract

Ce^{4+} cations are commonly used as electron acceptors during the water oxidation to O_2 reaction over Ir- and Ru-based catalysts. They can also be reduced to Ce^{3+} cations by excited electrons from the conduction band of an oxide semiconductor with a suitable energy level. In this work, we have studied their interaction with a rutile TiO_2(110) single crystal upon band gap excitation by femtosecond transient absorption spectroscopy (TAS) in solution in the 350–900 nm range and up to 3.5 ns. Unlike excitation in the presence of water alone the addition of Ce^{4+} resulted in a clear ground-state bleaching (GSB) signal at the band gap energy of TiO_2 (ca. 400 nm) with a time constant $t = 4$–5 ps. This indicated that the Ce^{4+} cations presence has quenched the e-h recombination rate when compared to water alone. In addition to GSB, two positive signals are observed and are attributed to trapped holes (in the visible region, 450–550 nm) and trapped electrons in the IR region (>700 nm). Contrary to expectation, the lifetime of the positive signal between 450 and 550 nm decreased with increasing concentrations of Ce^{4+}. We attribute the decrease in the lifetime of this signal to electrostatic repulsion between Ce^{4+} at the surface of TiO_2(110) and positively charged trapped holes. It was also found that at the very short time scale (<2–3 ps) the fast decaying TAS signal of excited electrons in the conduction band is suppressed because of the presence of Ce^{4+} cations. Results point out that the presence of Ce^{4+} cations increases the residence time (mobility) of excited electrons and holes at the conduction band and valence band energy levels (instead of being trapped). This might provide further explanations for the enhanced reaction rate of water oxidation to O_2 in the presence of Ce^{4+} cations.

* Author to whom any correspondence should be addressed.

Supplementary material for this article is available online

Keywords: Rutile TiO_2(110) single crystal,
femtosecond transient absorption spectroscopy (TAS), Ce^{4+} cations interaction,
cerium ammonium nitrate (CAN), lifetime of excited electrons, hole traps, excited electron traps

1. Introduction

The study of electron transfer at the solid electrolyte interface offers much information related to redox reactions in which the solid donates or receives electrons from the electrolyte [1]. While the electrolyte interacts mostly with the surface of a solid, the latter bulk properties may determine the reaction rate in addition to that of the surface [2]. In the case of oxide semiconductors in the presence of photons with energy above their band gap energy, two types of reactions may occur depending on thermodynamics. A reaction can occur spontaneously ($-\Delta G$), in which the solid acts as a catalyst, hydrocarbon combustion for example [3], or it can have a $+\Delta G$, such as the water splitting reaction [4]. In the latter situation, the electron transfer reaction is further complicated because of the reverse reaction. To this end, decoupling the oxidation and reduction steps of the reaction has been pursued. It is worth mentioning that in nature the water splitting reaction is decoupled [5].

One such system is that of the interaction of an oxide semiconductor with metal cations [6]. The metal cation can either donate or accept electrons from the semiconductor depending on its redox potential. One of the early metal cations used together with the semiconductor under photo-excitation is a system composed of TiO_2 (*n*-type semiconductor) and Ce cations [7–9]. Since then many have investigated such a system, mostly in the solid state, however [10, 11].

This reaction can be presented as follows.

Upon the absorption of a photon with energy higher than the band gap energy ($h\Delta > E_{BG}$), electrons (e) and holes (h) are created in the conduction band (CB) and valence band (VB), respectively

$$TiO_2 \rightarrow h + e. \tag{1}$$

In the presence of protons and Ce^{3+} cations, holes are consumed and consequently, Ce^{4+} cations are formed together with the generation of H_2.

$$2Ce^{3+} + 2h + 2H^+ \rightarrow 2Ce^{4+} + H_2. \tag{2}$$

In the presence of water and Ce^{4+} cations, excited electrons are consumed and consequently, Ce^{3+} cations are formed and O_2 is generated.

$$4Ce^{4+} + 4h + 2H_2O \rightarrow 4Ce^{3+} + O_2 + 4H^+. \tag{3}$$

The redox potential of Ce^{4+}/Ce^{3+} is 1.45 V at pH = 0 (with respect to the reference AgCl electrode or ca. 1.7 V with respect to the reference hydrogen electrode, RHE) [12–14]. Considering that the rutile TiO_2 has a band gap of 3.0 eV and that its valence band is about 2.5 eV below RHE then both mechanisms are possible (reduction of Ce^{4+} cations at the conduction band and oxidation of Ce^{3+} at the valence band).

Cerium cations in solution are solvated with the nature of ligands dependent on the initial salt composition and the solution pH. In the case of Ce^{4+} cations from cerium ammonium nitrate (CAN), results pointed out that perfectly soluble Ce^{4+} cations are surrounded by water molecules in addition to the NO_3^- group. One such compound was identified as $(H_2O)_6Ce_2O(NO_3)_6$ and would exist in an oxo-dimer form ($Ce^{4+}-O-Ce^{4+}$) [15].

Both Ce^{4+} and Ce^{3+} cations have been successfully used as electron acceptors and electron donors upon the photo-excitation of TiO_2-based catalysts [7–9]. Also, the use of Ce^{4+} in CAN has been shown to be active as an electron acceptor for water oxidation using Ir-, or Ru-based catalysts [16–18] in their homogeneous systems as well as over Ir/TiO_2, Ru/TiO_2, and $Au\text{-}Pd/TiO_2$ for the same reaction [19, 20] in the absence of photons. The interaction of the complex (in the case of CAN) with the catalyst surface under photo-excitation is not known.

Pump-probe femtosecond transient absorption spectroscopy (TAS) is very useful in monitoring charge carriers in semiconductors in general upon light excitation [21–24]. In the case of TiO_2, numerous works have identified transient signals upon UV excitation [25–27]. These may be grouped into three sets of signals in the UV, visible, and infrared regions: (i) bleaching at the band gap energy position (called ground state bleaching, GSB), (ii) visible light absorption [28] and (iii) near-infrared to mid-infrared light absorption [29] (both called photon induced absorption). The GSB is due to a decreasing population of available electrons in the valence band upon light excitation, the visible response is largely attributed to signals originating from holes while the near-infrared to mid-infrared signals are due to deep and shallow trapped excited electrons near the conduction band as well as self-trapped excited electrons (polarons).

While many pump-probe femtosecond TAS studies have been conducted on powder oxide semiconductors, one of the main issues in photocatalysis is the effect of the state of the material. That is because the catalytic performance changes with the crystallite and particle sizes, with the degree of crystallinity [30], and with the extent of bulk defects (largely viewed as oxygen vacancies and interstitial metal atoms [31], such as the Magneli phase [32]) among other factors). While all will share largely the same main characteristics (similar band gap energy for example) changes in the lifetime of the

excited charge carriers, from one system to the other, prevent extracting fundamental information that may be used as a reference. This is best done using a single crystal because the surface orientation and bulk structure have a higher chance of being reproduced. This is in addition to the absence of grain boundaries which also affect e-h generation and recombination [33, 34]. Rutile TiO_2(110) single crystal is the most understood prototype oxide semiconductor and probably the most stable. This is largely because of its relatively high electronic conductivity which has allowed for a myriad of electron spectroscopy and microscopy studies to be conducted for over three decades [35–37].

While there is an increasing number of pump-probe TAS on single crystals [38–40], we are not aware of any in solution under photoexcitation in the presence of metal cations as electron acceptors. In principle, one would expect that electron acceptors would decrease the population of excited electrons and increase those of holes. We found that, at the picosecond to nanosecond scale this is not the case and that the interaction leads to a more complex situation. At a short time (<3 ps) the near infra-red signals increased and the longer decay time of the visible region (up to 2 ns), often considered as resulting from holes, became much shorter when Ce^{4+} cations were present.

2. Experimental

TAS measurements were conducted on 0.1 ps to 3.5 ns timescales. The system is based on a regeneratively amplified Ti: sapphire laser system that produces 800 nm laser pulses of 90 fs pulse width at 1 kHz repetition rate and in conjunction with Excipro pump-probe spectrometers (Moscow). More details on the system can be found in [31]. Briefly, the pump pulses at 340 nm were generated after passing through 90% of the 800 nm beam into a spectrally tuneable (240 − 2600 nm) optical parametric amplifier (TOPAS Prime, Spectra-Physics) and a frequency mixer (NIR vis UV, Light conversion). The fluency of the pump power was adjusted by using neutral density filters to avoid multiple exciton generation (it was about 15 mW cm^{-2}). To generate the probe pulses (UV, visible and NIR wavelength continuum) the remaining 10% of the 800 nm amplified pulses were focused onto a 2 mm thick CaF_2 crystal. The pump pulses (340 nm) were overlapped on the TiO_2 (110) single crystal and then reflected with a mirror to the detector (figure S2). The pump pulses passed through a synchronized chopper (500 Hz) which blocked alternative pump pulses. The TAS experiments were carried out in a home-made reactor constructed around a standard 10 mm optical path quartz cuvette. The rectangular shape fresh TiO_2 single crystal 10 × 5 mm^2 was inserted into a slotted sample holder (3D printed in-house). The sample holder was placed inside the cuvette. The sample was positioned vertically, normal to the pump/probe laser beams, enabling the TAS measurements in the reflection mode. The cuvette was filled with deionized water (Milli Q filtration) and sealed with a re-closable plastic cap with rubber seal (3D printed in-house). The cap was equipped with two standard syringe needles for N_2 purging and introduction of the reactants. Two polypropylene tubes were attached to the needles and were equipped with clamp seals to control the gas phase and introduction of reactants. Ceric ammonium nitrate was dissolved in water to 1.3×10^{-3} M concentration i.e. 100 mg in 100 ml at room temperature. After complete dissolution Ce solution was added to the reactor drop-wise with microliter droplet volume through one of the needles by a syringe. The change in absorption (ΔA) of the excited state is calculated by subtracting the absorption of the excited from the unexcited sample.

3. Results

Figure 1 presents the TAS signal in the UV and visible regions. Figures 1(A) and (B) shows the results when CAN was present in the reactor at the indicated concentration. In previous work, it was reported that in order to avoid interferences due to the yellow color of CAN low concentrations are needed [8]. These were in the order x mM and were found to be adequate to trap electrons and consequently release O_2 from water (equation (3)). In this work, we have used many orders of magnitudes lower concentrations because of the small area of the single crystal (0.5 cm^2). A CAN concentration of 10^{-4} mM contains about 10^{16} atoms of Ce^{4+} cations, which is ten to twenty times more than Ti cations on the surface. The negative signal just below 350 nm is due to the laser excitation (340 nm). At about 1–2 ps a negative peak appears with a minimum close to 385 nm which is above the band gap energy of the rutile TiO_2. The signal disappearance by about 3 ps is followed by a broader negative peak at the band gap energy of TiO_2 (attributed to GSB) due to a decreased population of electrons in the valence band. This is taken as evidence of an excited system where a non-negligible fraction of electrons was exited to the conduction band (and traps). After the recovery of the signal, a rise (a positive signal) from 450–550 nm is seen (PIA). This signal is commonly viewed as due to hole traps, because of its energy (about 2.5 eV). Although this may not be the only reason, deep-trapped electrons may also be excited to the conduction band at this energy level. Figure 1(C), in the presence of water alone, shows a similar pattern. The first decay occurs at the same wavelength as in the presence of CAN (385 nm) and disappears at the same time. The GSB at 410 nm and the rise above 450 nm while present are barely noticeable. This indicated that the same phenomenon occurs in the absence of Ce^{4+} but with a much lower intensity. The same experiment was conducted in an aprotic system (*n*-heptane in this case) in order to remove the contribution of the signal related to protons interaction with the surface (figure S1). While the TiO_2 surface in an aqueous environment is fully hydroxylated, it is not expected to be in the *n*-heptane phase. Very similar behavior to that observed for water, except that the negative peak at about 2 ps has shifted further down by about 20 nm. The photoionization threshold of water occurs at

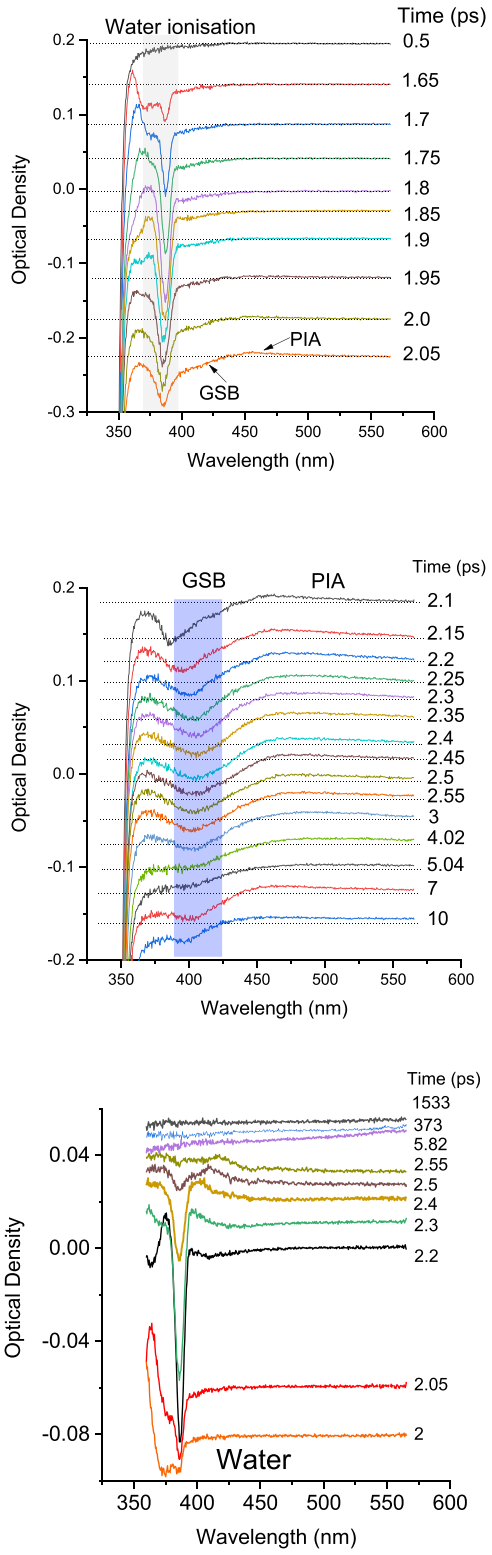

Figure 1. Pump-probe femtosecond TAS in the UV and visible regions of a TiO_2(110) rutile single crystal in an aqueous solution with ceric ammonium nitrate, CAN (1.08×10^{-4} mM) (A) and (B) and in the absence of the CAN (C). PIA: photon-induced absorption; GSB: ground state bleaching.

about 6.5 eV [41]. Previous work has shown that water [42] as well as hydrocarbon [43, 44] can lead to a TAS signal upon the absorption of two photons. Also, in the case of *n*-heptane, it was reported that photodissociation to C_3 and C_4 fragments [45] occurs at energies above 2 eV. We attribute the signals at 385 nm and 365 nm to the presence of water and *n*-heptane, respectively.

Figure 2(A) presents the kinetics of the spectra of figures 1 and S1 at 500 nm up to 2000 ps. The presence of CAN has resulted in a faster disappearance of the signal (which is commonly attributed to hole traps). This signal was the longest in an aprotic solvent while that of water was in between. The signal was fitted with a bi-exponential decay function with its parameters presented in table 1.

The first component (A_1t_1) was the most affected where it decreased two orders of magnitudes from heptane to CAN. The average time constant $<t>$ decreased from 7.7 ns to 132 ps. Considering that CAN provides Ce^{4+} cations it is not viewed as a hole trap element as it is rather an electron acceptor. Therefore, the clear decrease in the lifetime of the signal at 500 nm may not be solely attributed to holes or that the interaction of CAN with the surface of TiO_2 affects it differently (see discussion section). Figures 2(B) and (C) presents the rising part of the bleaching signal at 410 nm for two CAN concentrations (2 and 3×10^{-4} mM). The shape is similar in both cases which could be fit with a single exponential function. The extracted time constant is slightly higher (5.4 ps) for 3×10^{-4} mM CAN than that of the 2×10^{-4} mM CAN (4.5 ps). In summary, in this section, it can be stated that while the addition of CAN increases the population of electron transfer from the valence band to the conduction band (GSB) it is seen to considerably decrease the lifetime of the visible TAS signal.

Figure 3 presents the TAS signal in the visible and near-infrared regions in the three environments (CAN, water, and *n*-heptane). The exact shape of the signal may not bring much information because it is affected by the quality of the white light as much as the crystal's optical properties and bulk electronic structure in addition to the experimental parameters such as the exact spot on the crystal and the slight changes due to adjustment of the optical density filters from one experiment to the other. It is however composed of patterns that are reproducible on a TiO_2 (110) single crystal. These are presented by arrows in the figure (a similar shape is obtained in air [31, 39]). The TAS decay of three wavelengths (720 nm, 820 nm and 870 nm) for the series was plotted and fitted with a bi-exponential function from which the average time constants are obtained (table S1). It appears that the average time constant is higher for the 870–900 nm when compared to the 720 nm decay signal. It is also clear that the addition of CAN decreased the time constant although it is not possible to extract quantitative analyses tracking the CAN concentration.

There is however one clear trend at very short time, figure 4. Figures 4(A)–(E) presents the un-normalized TAS signal at five different wavelengths. This is the same time range as that of the initial recovery of the GSB signal shown in figure 2. There is very little difference between the TAS signal obtained in water and that obtained in the presence of 1.8×10^{-5} mM of CAN (figures 4(A) and (B)). In previous work[31], we obtained a similar trend in the gas phase for a fresh TiO_2(110)

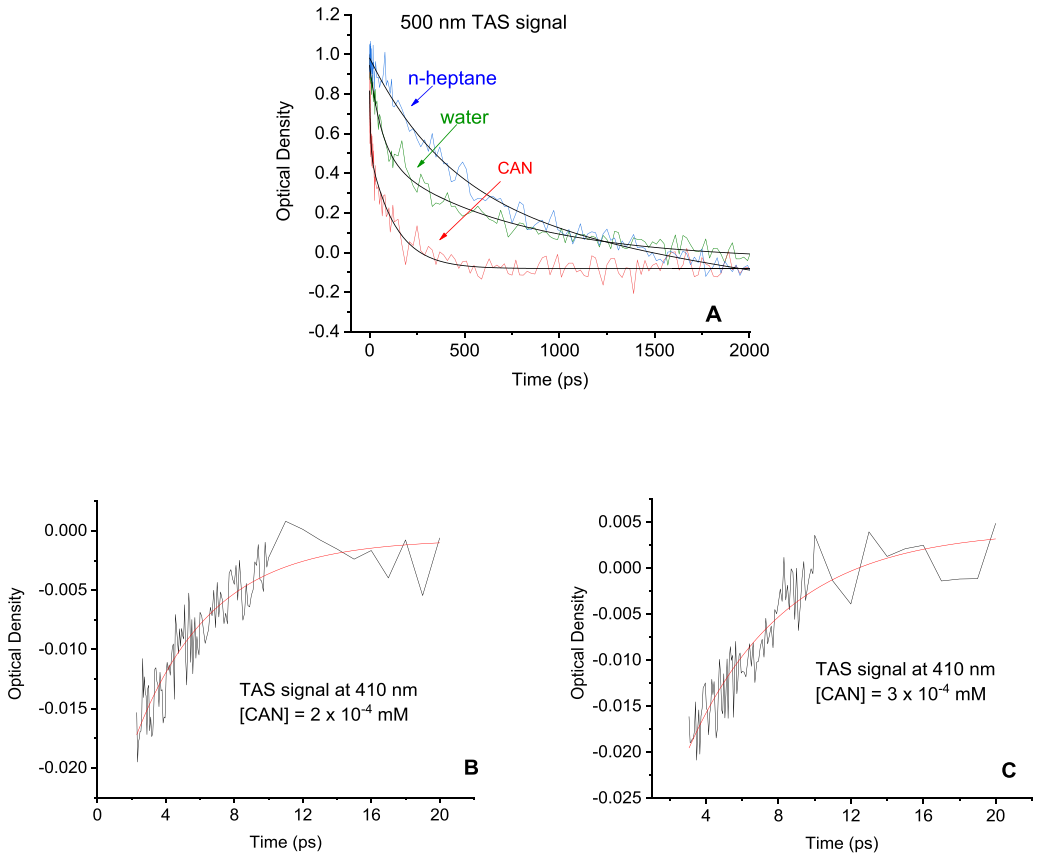

Figure 2. Normalized TAS decay of the signal at 500 nm of TiO_2 (110) rutile single crystal in the presence of *n*-heptane, water, and CAN (1.08×10^{-4} mM) (A). The black solid lines are for the bi-exponential function used to fit the data; $A_1\exp(-x/t_1) + A_2\exp(-x/t_2)$ (table 1). TAS 410 nm recovery of the bleaching signal in the presence of CAN at 2×10^{-4} mM (B), and 3×10^{-4} mM (C). The red solid lines in (B) and (C) are for the single exponential function used to fit the data (table 2).

Table 1. Parameters of the bi-exponential function fitting for the 500 nm of TiO_2(110) rutile single crystal TAS decay signal in *n*-heptane, water and CAN solutions. Statistical R^2 values are included.

Parameters	*n*-heptane	Water	(CAN) = 1.08×10^{-4} mM
A_1	0.77	0.45	0.31
t_1 ps	433	65.2	5.8
A_2	1.37	0.53	0.6
t_2 ps	7977	719	135
$<t>$ ps	7754	672	132
R^2	0.99	0.99	0.96

Table 2. Parameters for the single exponential function used to fit the recovery part of the bleaching signal at 410 nm of TiO_2(110) rutile single crystal in the presence of CAN solutions at the indicated concentrations; figure 2. Statistical R^2 values are included.

Parameters	(CAN) = 2×10^{-4} mM	(CAN) = 3×10^{-4} mM
A	−0.03	−0.04
t ps	4.5	5.4
R^2	0.84	0.85

single crystal. After the very fast rise, there is a sharp decay of the signal within a ps followed by a much slower decay. This behavior is not the same for all regions in the 700–900 nm. The sharp decay is more pronounced at higher wavelengths.

Increasing CAN concentrations to 1.08 and 2×10^{-4} mM affected the fast decay component of the signal and at 3×10^{-4} mM, the decay was much slower (figure 4(E)). In order to monitor the differences normalized spectra of the signal at the different CAN concentrations are plotted in figure 4(F). The sharp decay of the signal around 830 nm is attenuated in the presence of CAN. A bi-exponential function fitted well the TAS signal, with the average time constant increased from 0.1 ps to 27.8 ps (table 3).

4. Discussion

The main observed points in the study are the following.

1. A GSB signal (at the band gap energy) is seen when CAN concentration was 1.08×10^{-4} mM and above.
2. The TAS lifetime signal at 500–550 nm decreases in the presence of CAN, when compared to water or *n*-heptane.

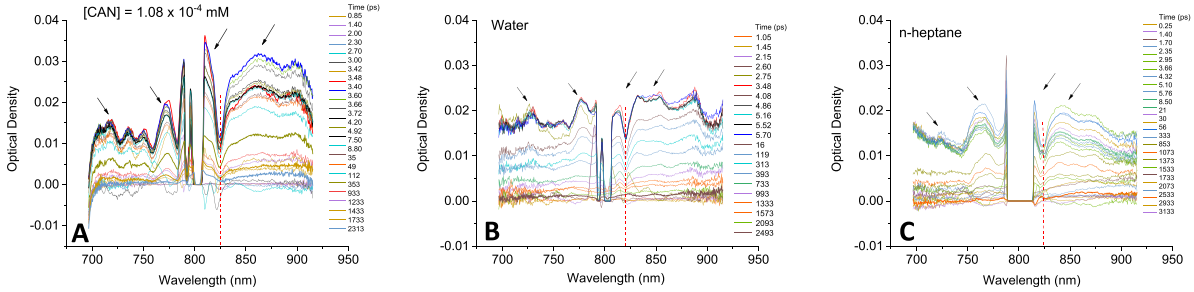

Figure 3. Pump-probe femto second TAS signal in the visible and near-infrared regions of TiO_2(110) rutile single crystal in an aqueous solution with ceric ammonium nitrate (A), water (B) and in an aprotic medium of *n*-heptane (C).

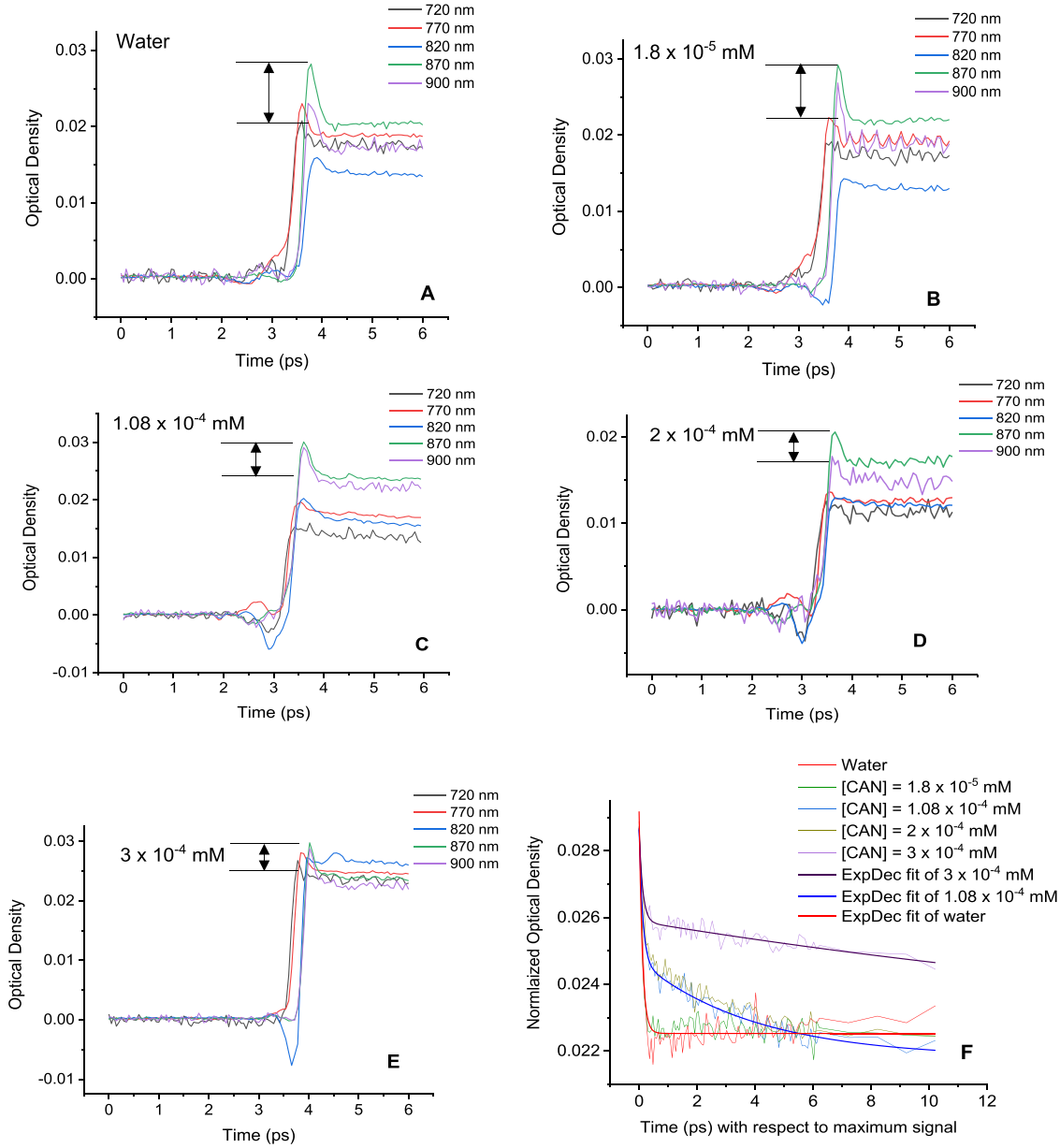

Figure 4. Un-normalized TAS decay of the signal of TiO_2(110) rutile single crystal in the presence of water, and CAN. (A) water, (B) 1.8×10^{-5} mM, (C) 1.08×10^{-4} mM, (D) 2×10^{-4} mM, and (E) 3×10^{-4} mM. (F) 0–10 ps TAS decay of the signal at 830 nm in the presence of water, and CAN at the indicated concentrations. The solid lines in (F) are for the bi-exponential function used to fit the data (table 3). The time in (F) is with respect to the max signal (0 ps) which is about 4 ps in (A)–(E) to simply the fitting. The scale bar, represented by a vertical double arrow and two horizontal lines for the 870 nm signal are a guide to eye to highlight the change in the response with increasing CAN concentrations.

Table 3. Parameters for the bi-exponential function fitting for the 830 nm TAS decay signal of TiO_2(110) rutile single crystal in the presence of water and CAN solutions presented in figure 4(F). Statistical R^2 values are included.

Parameters	Water	(CAN) = 1.08 × 10^{-4} mM	(CAN) = 3 × 10^{-4} mM
A_1	0.0036	0.0039	0.0028
t_1 ps	0.11	0.12	1.2
A_2	0.0031	0.0029	0.0041
t_2 ps	0.11	4.0	28.56
$<t>$ ps	0.11	3.85	27.80
R^2	0.85	0.96	0.89

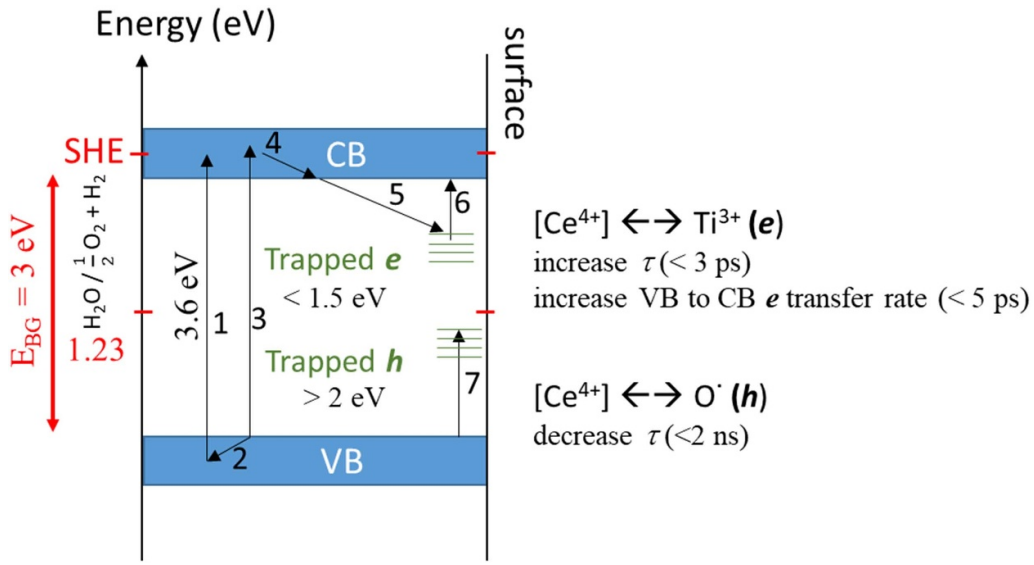

Figure 5. Schematic representation of the Ce^{4+} interaction with the surface of TiO_2(110) events as probed by TAS. E_{BG}: band gap energy of rutile TiO_2; VB: valence band; CB: conduction band. τ: average time constants (tables 1–3). Arrows indicate the direction of electron transfer. In the case of hole transfer, the arrow direction would be reversed. While TiO_2 is an *n*-type semiconductor with an upward bend bending, this is neglected because the effect of CAN is not known. Water splitting redox potential is indicated (1.23 eV e^{-1}) in red. Numbers 1–6 are described in the text.

3. The decay in the TAS signal in the 700–900 nm is not homogenous. At long lifetime, there is no noticeable difference in the presence or absence of CAN. Yet, at a short time (up to 3–5 ps) the presence of CAN (with concentration equal to 1.08 × 10^{-4} mM and above) increased the lifetime of the decay.

CAN in solution is in the form of Ce^{4+} cations, solvated Ce^{4+} or a complex of the form indicated in the introduction section. The surface of TiO_2(110) in aqueous environment is fully hydroxylated [46]. Surface hydroxyls are not good centers for hole trapping [47], yet the presence of water makes them more active centers for hole trapping [48]. Exited electrons are trapped at Ti cations centers with different energies extending from a fraction of an eV up to 1.5 eV and probably higher. This is often referred to as shallow and deep traps. Knowing that electron transfer from the surface to Ce^{4+} cations to reduce them to Ce^{3+} cations is slower than the investigated time in this work, the observed differences in the visible and near-infrared regions may not be linked to the complete electron transfer. They are to be viewed as due to the interaction of CAN with the surface of the single crystal.

Figure 5 presents an energy diagram in which we attempt to rationalize the results. First, we describe the events. The TiO_2(110) single crystal in aqueous solution is excited with a 3.6 eV laser, this leads to electronic excitation from levels below the edge of the VB (largely O2p) to levels above the edge of the CB (1). Some electrons from higher levels in the VB relax to trap the newly formed hole, before being excited to the CB (2) or directly excited to the CB (3). These excited electrons would move to the edge of the CB (4) and then be trapped in shallow and deep sites in the mid-gap (5). Excitation of these trapped electrons back to the conduction band then occurs and these are monitored in the 700–900 nm in this work (6). The initial decay in TiO_2(110) in water is very fast (ca. 0.1 ps) and followed by a much slower one (hundreds of ps). In the presence of Ce^{4+}, the very fast decay is slowed down and has two components (1.2 ps and 27 ps) at 3 × 10^{-4} mM. This is then seen as due to the stabilization of these trapped

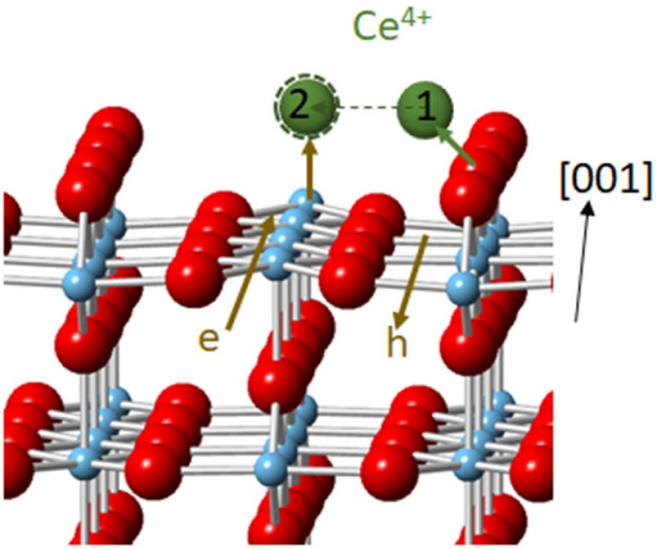

Scheme 1. A pictorial representation of the interaction of Ce^{4+} cations with the surface of TiO_2(110) single crystal before (1) and after (2) photon excitation. Water is not drawn for simplicity and because its role in solvating the ion is not clear. In the ground state, Ce^{4+} is attracted to surface oxygen anions and repelled from Ti cations. Upon light excitation, electrons flow from oxygen anions (mostly O_{2c}) to Ti cations. This results in the Ti^{3+} (excited electrons) and $O^{\cdot}_{2c}$ (holes). As a result, Ce^{4+} cations will move closer to Ti^{3+} cations (2). The continuation of the process with other Ce cations will result in a flow of excited electrons—attraction (in this case along the [001] direction [52, 53]) and holes will revert their path—repulsion. This may explain the increased lifetime of excited electrons at the CB and the decreased lifetime of trapped holes. Red: O anions, blue: Ti cations; green: Ce cations. Arrows in brown are during excitation and in green for the ground state.

electrons at the surface and near surface. It might be due to the electrostatic interaction between the positively charged Ce^{4+} cations and the excited electrons. It has been shown in other work that electron polarons in TiO_2 are affected by the presence of surface adsorbates by STM and DFT + U computation for example [49–51]. The decrease in the lifetime of the TAS signal at 500 nm (7) is rationalized as due to the destabilization of trapped holes at and near the surface by the presence of Ce^{4+}; electrostatic interaction where repulsion may occur between the positively charged holes (in the mid-gap region) and Ce^{4+} cations.

4.1. A plausible explanation, based on ground state adsorption and excited state reaction

The reason for this can be linked to the difference between the ground state and excited state of both Ce^{4+} cations and the surface of TiO_2 (scheme 1). Ce^{4+} cations close to the surface would feel the electronic charge density around the surface oxygen atoms because the latter are negatively charged. These surface oxygen atoms are centers for hole traps in the excited state. The sites that are surrounded by Ce^{4+} cations are not centers for hole traps anymore (due to repulsion). Also, because they are stabilized (electrostatically) on the surface, they attract excited electrons from the Ti3d states, destabilizing their trap centers. This makes excited electrons more mobile (more metallic) at the surface and holes more mobile in regions where Ce^{4+} are not adsorbed on the surface oxygen as well as in deeper layers.

Within the context of electron transfer in water splitting in the presence of photons and Ce^{4+} cations, the interaction of the latter with the surface of rutile TiO_2 may have two positive consequences. First, the interaction stabilizes excited electrons in the conduction band (instead of being trapped) and therefore makes them energetically more favorable for the electron transfer to occur. Second, they destabilize trapped holes (residing in the mid-gap state [54, 55]) back to the VB which also results in a faster hole transfer to adsorbed water (or hydroxyls) due to the increased energy difference between the redox potential of water (1.23 eV) and the valence band of rutile TiO_2 (3 eV) instead of the mid-gap state (2 eV).

5. Conclusions

The interaction of Ce^{4+} cations (from, CAN) and rutile TiO_2(110) single crystal is studied by femtosecond TAS in solution in the 350–900 nm range and up to 3.5 ns. A negative signal at the band gap energy of TiO_2 (400–410 nm) is found in the presence of Ce^{4+}. This is attributed to GSB. The lifetime of the positive signal between 450 and 550 nm decreases with increasing concentrations of Ce^{4+}. We explain the decrease in the lifetime of this signal, largely attributed to holes, as due to electrostatic repulsion between Ce^{4+} at the surface of TiO_2(110) and positively charged trapped holes. This results in hole de-trapping back to the valence band. This may enhance water splitting to O_2 because of the increased energy difference between the redox potential of water and the hole energy at the valence band. It was also found that at the very short time scale (<2–3 ps) the fast decaying TAS signal of CB excited electrons is suppressed because of the presence of Ce^{4+} cations. This is explained as due to the electrostatic attraction between Ce^{4+} cations and excited electrons at the CB preventing them from being trapped in deeper layers. It is thus postulated that the presence of Ce^{4+} cations makes excited electrons and holes more mobile at the CB and VB energies, which would enhance water oxidation to O_2.

Data availability statement

All data that support the findings of this study are included within the article (and any supplementary files).

ORCID iD

H Idriss https://orcid.org/0000-0001-8614-7019

References

[1] Bard A J and Faulkner L R 2001 Electrochemical methods *Fundamentals and Applications* 2nd edn (Wiley)
[2] Qiu J, Wu M, Luo W, Xu B, Liu G and Ouyang C 2021 *J. Phys. Chem.* C **125** 23510–20

[3] Osterloh F E 2017 *ACS Energy Lett.* **2** 445–53
[4] Fujishima A and Honda K 1972 *Nature* **238** 37–38
[5] Barber J 2017 *Nat. Plants* **3** 1–5
[6] Su R *et al* 2016 *ACS Catal.* **6** 4239–47
[7] Bamwenda G R, Uesigi T, Abe Y, Sayama K and Arakawa H 2001 *Appl. Catal.* A **205** 117–28
[8] Kozlova E A, Korobkina T P and Vorontsov A V 2009 *Int. J. Hydrog. Energy.* **34** 138–46
[9] Kozlova E A, Korobkina T P, Vorontsov A V and Parmon V N 2009 *Appl. Catal.* A **367** 130–7
[10] Mishra M K, Callejas J F, Pacholski M L, Ciston J, Okrut A, Kumar R, Van Dyk A, Barton D G, Bohling J C and Katz A 2021 *ACS Appl. Nano Mater.* **4** 11590–600
[11] Buchanan C A, Herrera D, Balasubramanian M, Goldsmith B R and Singh N 2022 *JACS Au* **2** 2742–57
[12] Pletcher D and Valves E M 1988 *Electrochim. Acta* **33** 499–907
[13] Wei Y, Fang B, Aral T and Kumagai M 2005 *J. Appl. Electrochem.* **35** 561–6
[14] Wadsworth E, Duke F R and Goetz C A 1957 *Anal. Chem.* **29** 1824–5
[15] Demars T J, Bera M K, Seifert S, Antonio M R and Ellis R J 2015 *Angew Chem., Int. Ed.* **54** 7534–8
[16] Hong D, Murakami M, Yamada Y and Fukuzumi S 2012 *Energy Environ. Sci.* **5** 5708–16
[17] Menendez R G, Bucci A, Hutchinson R, Bellachioma G, Zuccaccia C, Idriss H and Macchioni A 2016 *ACS Energy Lett.* **2** 105–10
[18] Gersten S W, Samuels G L and Meyer T J 1982 *J. Am. Chem. Soc.* **14** 4029–30
[19] Wahab K A and Idriss H 2024 *Catalysts* **14** 87
[20] Alrushaid M, Wahab K A, Nadeem M A and Idriss H 2021 *Catalysts* **11** 1030
[21] Norris P M, Caffrey A P, Stevens R J, Klopf J M, McLeskey J T Jr and Smith A N 2003 *Rev. Sci. Instrum.* **74** 400–6
[22] Sundaram S K and Mazur E 2002 *Nat. Mater.* **1** 217–24
[23] Zhang Y, Dai J, Zhong X, Zhang D, Zhong G and Li J 2021 *Adv. Sci.* **8** 2102488
[24] Prasankumar R P, Upadhya P C and Taylor A J 2009 *Phys. Status Solidi* b **246** 1973–95
[25] Yamakata A, Vequizo J J M and Matsunaga H 2015 *J. Phys. Chem.* C **119** 24538–45
[26] Chu W, Saidi W A, Zheng Q, Xie Y, Zhenggang L, Prezhdo O V, Hrvoje Petek H and Zhao J 2016 *J. Am. Chem. Soc.* **138** 13740–9
[27] Tamaki Y, Furube A, Murai M, Hara K, Katoh R and Tachiya M 2007 *Phys. Chem. Chem. Phys.* **9** 1453–60
[28] Onda K, Li B, Zhao J, Jordan K D, Yang J and Petek H 2005 *Science* **308** 1154–8
[29] Triggiani L, Brunetti A, Aloi A, Comparelli R, Curri M L, Agostiano A, Striccoli M and Tommasi R 2014 *J. Phys. Chem.* C **118** 25215–22
[30] Wahab A K, Ould-Chikh S, Meyer K and Idriss H 2017 *J. Catal.* **352** 657–71
[31] Al-Amoudi M, Katsiev K and Idriss H 2023 *J. Phys. Chem. Lett.* **14** 9238–44
[32] Zhang Q, Liu W, Zhou Y, Li J, Sun T, Liu Q, Ma Y, Wang J, Li J and Zhao R 2021 *Z. Anorg. Allg. Chem.* **647** 126–33
[33] Gao Z, Leng C, Zhao H, Wei X, Shi H and Xiao Z 2024 *Adv. Mater.* **36** 2304855
[34] Wrana D, Gensch T, Jany B R, Cieślik K, Rodenbücher C, Cempura G, Kruk A and Krok F 2021 *Appl. Surf. Sci.* **569** 150909
[35] Connelly K A and Idriss H 2012 *Green Chem.* **14** 260–80
[36] Diebold U 2003 *Appl. Phys.* A **76** 681–7
[37] Thomas A G and Syres K L 2012 *Chem. Soc. Rev.* **41** 4207–17
[38] Argondizzo A, Cui X, Wang C, Sun H, Shang H, Zhao J and Petek H 2015 *Phys. Rev.* B **91** 1–10
[39] Maity P, Katsiev K, Mohammed O F and Idriss H 2018 *J. Phys. Chem.* C **122** 8925–32
[40] Katsiev K, Harrison G, Thornton G and Idriss H 2019 *ACS Catal.* **9** 8294–305
[41] Nikogosyan D N, Oraevsky A A and Rupasov V I 1983 *Chem. Phys.* **77** 131–43
[42] Migus A, Gauduel Y, Martin J L and Antonetti A 1987 *Phys. Rev. Lett.* **58** 1559–62
[43] Rasmusson M, Tarnovsky A N, Åkesson E and Sundström V 2001 *Chem. Phys. Lett.* **335** 201–8
[44] Bowman R M, Lu H and Eisenthal K B 1988 *J. Chem. Phys.* **89** 606–8
[45] Chen J-H, Dunbar R C and Chen J-H 1986 *Int. J. Mass Spectrom. Ion Process.* **72** 115–23
[46] Sasahara A, Murakami T and Tomitori M 2018 *Surf. Sci.* **668** 61–67
[47] Fazio G, Ferrighi L and Di Valentin C 2016 *Nano Energy* **27** 673–89
[48] Di Valentin C, Pacchioni G and Selloni A 2006 *Phys. Rev. Lett.* **97** 166803
[49] Reticcioli M, Diebold U and Franchini C 2022 *J. Phys.: Condens. Matter* **34** 1–8
[50] Reticcioli M, Sokolović I, Schmid M, Diebold U, Setvin M and Franchini C 2019 *Phys. Rev. Lett.* **122** 016805
[51] Gao C, Zhang L, Zheng Q and Zhao J 2021 *J. Phys. Chem.* C **125** 27275–82
[52] Byl O and Yates J T 2006 *J. Phys. Chem.* B **110** 22966–7
[53] Williams O B J, Baek B, Harrison G T, Katsiev K, Thornton G and Idriss H 2022 *J. Am. Chem. Soc.* **144** 1034–44
[54] Shirai K *et al* 2018 *J. Am. Chem. Soc.* **140** 1415–22
[55] Di Valentin C and Selloni A 2011 *J. Phys. Chem. Lett.* **2** 2223–8